B. G. Thomas*, R. Singh, S. P. Vanka, K. Timmel, S. Eckert and G. Gerbeth

Effect of Single-Ruler Electromagnetic Braking (EMBr) Location on Transient Flow in Continuous Casting

Abstract: Ultrasonic Doppler velocimetry measurements and large eddy simulations were conducted on a laboratory-scale physical model of a steel continuous slab caster with a low-melting alloy, both with and without an applied single-ruler magnetic field in one of two different vertical orientations. The computational model agreed very closely with the measurements in all respects, including time-averaged flow, velocity profiles, and transient velocity histories at specific locations. The magnetic field altered both the classic double-roll flow pattern and the flow stability. Lowering the magnetic field below the nozzle caused steeper downward jet angles, lower surface velocities, lower turbulent kinetic energy at the surface, and better flow stability, especially toward the surface, and at higher frequencies. The experimental and computational results both show that the electromagnetic field should not be placed with its maximum directly across the nozzle ports, where it may aggravate unstable flow.

Keywords: continuous casting, LES model, UDV measurements, EMBr, electromagnetic braking

PACS® (2010). 47.65.-d, 47.11.Bc, 47.27.E-, 47.27.ep 47.27.wg, 81.20.Hy

DOI 10.1515/jmsp-2014-0047
Received November 15, 2014; accepted December 6, 2014

1 Introduction

The quality of steel products is greatly affected by the fluid flow near the top surface of the mold during the continuous casting process. Maintaining stable flow conditions is well known to produce steel of the best quality, especially if the jet first impinges on the narrow face, and splits, flowing upward toward the free surface, and downward, generating a stable "double-roll" flow pattern [1, 2]. The flow pattern depends on the nozzle geometry, casting speed, mold width, mold thickness, argon gas injection, submergence depth, and the application of electromagnetic fields (EMFs). The highly turbulent nature of flow in the mold causes transient behavior even during statistically steady-state operation. Sudden large increases in velocity, level fluctuations, vortex formation, and other intermittent flow events can lead to the entrainment of mold slag, the formation of surface defects, and other quality problems. Magnetic fields are one of the few process parameters that respond to changes in the flow conditions and have been proposed as a means to stabilize mold flow [1–5].

In steel slab casting, both static and moving magnetic fields have been used and studied. Statically applied EMF configurations include local fields (circular fields on each side of the submerged entry nozzle (SEN) [6–10]), single-ruler fields (a rectangular field across the entire mold width [10–14]), and double-ruler fields (two ruler-shaped fields, with one positioned across the mold above the nozzle ports and the other across or below the nozzle ports [3, 5, 12, 15–17]). The flow of a conducting fluid such as steel through a magnetic field generates a force opposing the motion, and thus should be self-stabilizing. However, the magnetic field can change the flow stability in non-obvious ways [11–15].

The electrical conductivity of the walls, such as the solid steel shell that surrounds the liquid cavity in continuous casting, is an essential parameter affecting the flow when magnetic fields are active. Electrically conducting walls allow for a closure of the induced currents outside the liquid region [14], which has a dramatic effect on the Lorentz force distributions [13], and a stabilizing effect on the flow [11–15]. Recently, mold flow in a scaled physical model with GaInSn, a low melting liquid metal alloy, has been studied with ultrasonic Doppler velocimetry (UDV) measurements [11, 18] and large eddy simulations (LESs) [12–14] to investigate the effect of ruler electromagnetic braking (EMBr) on transient flow phenomena, with conducting (brass) versus insulated (plastic) side walls. The application of a single-ruler

***Corresponding author: B. G. Thomas,** Mechanical Science and Engineering, University of Illinois, 1206 West Green Street, Urbana, IL 61801, USA, E-mail: bgthomas@illinois.edu
R. Singh: E-mail: singh.ramnik14@gmail.com, **S. P. Vanka:** E-mail: spvanka@illinois.edu, Mechanical Science and Engineering, University of Illinois, 1206 West Green Street, Urbana, IL 61801, USA
K. Timmel: E-mail: k.timmel@hzdr.de, **S. Eckert:** E-mail: s.eckert@hzdr.de, **G. Gerbeth:** E-mail: g.gerbeth@hzdr.de, Helmholtz-Zentrum Dresden-Rossendorf, Dresden, Germany

EMBr over the nozzle with insulated walls made the mold flow unstable, with large-scale wobbling of the jets. With insulating walls, the current loops returning through the molten steel induce forces that deflect the local current-carrying flow, thus carrying the flow destabilizing effects to locations elsewhere through a complex feedback manner. This behavior is suppressed with conducting side walls, such as the solidifying steel shell of a real caster or the brass plates of the physical model. This is because the forces induced by current loops returning through the solid shell have no effect.

In the present study, two new LESs are performed of the mold flow in a laboratory-scale slab caster with conducting walls and a single-ruler magnetic field. The transient and time-averaged results of the two simulations are compared with the measurements. The results reveal important insights for the practical operation of commercial casters with EMBr.

2 Laboratory experiments

The geometry of the laboratory-scale caster, Mini-LIMMCAST – including the long, circular SEN with bifurcated round ports and the rectangular mold – is given in Figure 1 and Table 1. The round-bore nozzle is about 300 mm long (30 diameters), so that conditions at its

Table 1: Process parameters (Ga–In–Sn model).

Mold width	140 mm
Mold thickness	35 mm
Mold/strand length	330 mm
Nozzle port width/height	8 mm/18 mm
Nozzle port angle	0°
Nozzle bore inner/outer	10 mm/15 mm
SEN submergence depth (liquid surface to top of port)	72 mm
Total volume flow rate	110 ml/s
Bulk velocity at nozzle inlet	1.4 m/s
Casting speed	1.35 m/min
Thickness of shell (δ_{wall} at wide faces/narrow faces)	0.5 mm/0 mm
Kinematic viscosity (GaInSn)	0.34×10^{-6} m^2/s
Fluid density (GaInSn)	6360 kg/m^3
Conductivity of liquid (σ_{liquid})	3.2×10^6 1/Ωm
Conductivity of solid-steel-shell walls (σ_{wall})	15×10^6 1/Ωm
Wall conductance ratio ($C_w = 2\sigma_{wall}\delta_{wall}/\sigma_{liquid}L$)	0.13
Gas injection	No
Reynolds number (Re $= Ud_{inner}/\nu$, based on nozzle diameter)	41,180
Reynolds number (Re $= UL/\nu$, based on mold width)	9,860
Hartmann number (Ha $= BL\sqrt{\sigma/\rho\nu}$, based on mold width)	1,670
Froude number (Fr $= U/\sqrt{gL}$), based on mold width)	1.19
Stuart number (N $= B_0^2 L\sigma/\rho U$), based on mold width)	4.84
Cases	1. 92-mm EMBr 2. 121-mm EMBr

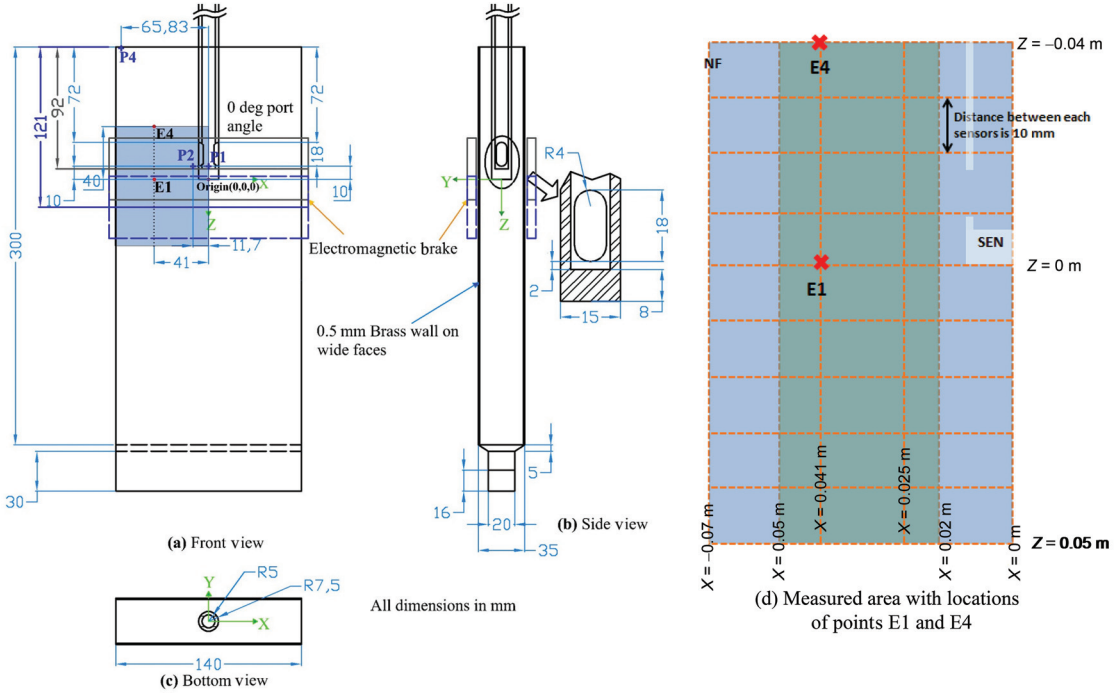

Figure 1: Schematic of Ga–In–Sn 1/6-scale laboratory model of slab caster with single-ruler EMBr.

top entrance – including the stopper rod tip and tundish outlet shape – have no effect on the fully developed flow produced toward its bottom. The mold has a horizontal cross section of 35 × 140 mm. The model geometry and conditions otherwise represent a 1/6 scale model of a 210 × 840 mm slab caster with a very deep, 432 mm nozzle submergence depth and 1.64 m/min casting speed [13]. This experimental facility operates with the liquid metal alloy Ga68In20Sn12, which is liquid at room temperature. The material properties of the alloy are reported by Plevachuk et al. [19].

The mold and the SEN are made of acrylic glass and represent by default electrically insulating boundary conditions. Metallic plates can be attached to the inner walls to emulate the electrical boundary condition of the solidifying steel shell in the real process. The plates are made of 0.5 mm brass. Considering a mold thickness $L = 35$ mm we get a wall conductance ratio $C_w = 2\sigma_w\delta_w/\sigma_f L$ (with σ_w and σ_f denoting the electrical conductivity of the wall and the fluid, respectively, whereas δ_w stand for the thickness of the electrically conducting walls) of about 0.13. Almost the same value arises for a steel caster with a mold thickness of 90 mm assuming a thickness of the solidified shell of 5 mm. In the experiment the brass plates cover the walls of the wide face. The narrow mold walls were left insulating in order to avoid any interference with the ultrasonic velocity measurements. This is not expected to have a significant effect on the resulting mold flow because the induced currents close in the Hartmann walls, which are perpendicular to the magnetic field lines (i.e. the wide walls).

This study considers the mold flow under the influence of a steady magnetic field in the form of a "single ruler"-type EMBr. The pole faces of the DC-magnet have a height of 40 mm and cover the entire mold width. Figure 2 shows the distribution of the magnetic field along the vertical casting direction for two positions of the EMBr. The position $z = 0$ corresponds to the lower end of the nozzle. More details about the three-dimensional measurements of the magnetic field distribution can be found in Timmel et al. [11, 18]. The single-ruler-shaped magnetic field has a major field component, which is parallel to the narrow mold face in Y-direction. The field strength is almost uniform across the width of the caster showing only a small descent at the narrow walls (maximum deviation about 5%) in Figure 2. Two positions of the EMBr are considered in this work to evaluate the effect of the field distance below the free surface liquid level in the mold: Case 92 mm EMBr, with maximum field strength directly across the center of the nozzle ports, and Case 121 mm EMBr, with maximum field strength lowered to below the SEN bottom (Figure 2). The nozzle ports are centered 92 mm below the top surface.

The velocity was measured with UDV using the DOP2000 velocimeter (model 2125, Signal Processing SA, Lausanne), which can operate up to ten ultrasonic transducers in a multiplexer mode. A linear array of ten 4

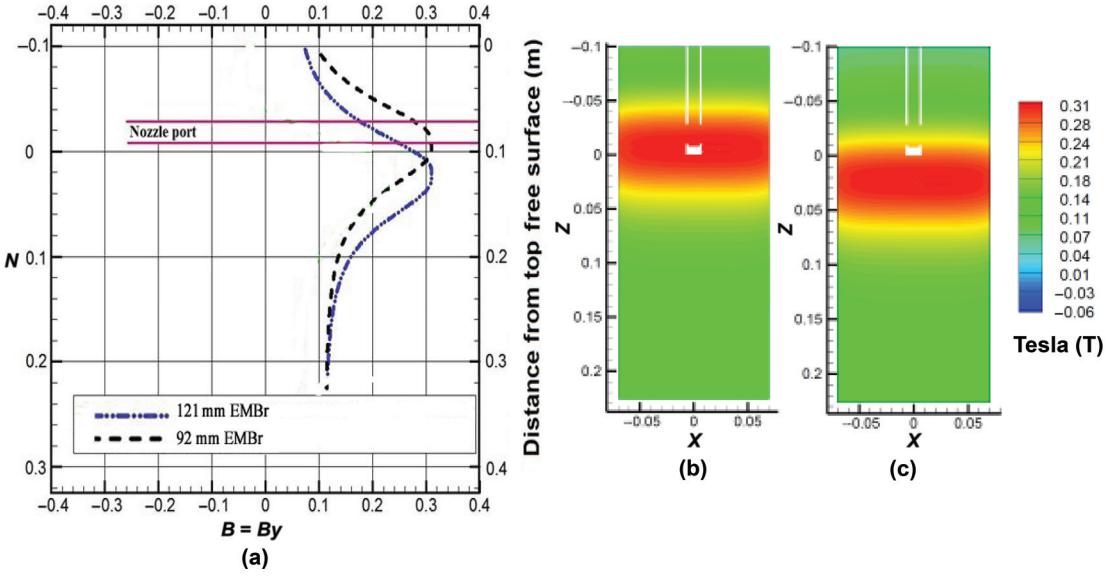

Figure 2: Two EMBr configurations with different vertical positions showing (a) profiles in vertical direction, and contour plots for (b) 92 mm case and (c) 121 mm case.

MHz transducers (TR0405LS, acoustic active diameter 5 mm) was attached at the narrow wall, measuring the horizontal velocity in the jet region. The transducers operate through the acrylic glass wall without interfering with the fluid flow. The spacing between the transducers is 10 mm, resulting in a total height of the measuring field of 90 mm, as shown in Figure 1(d). A more detailed description of the measurement method and procedure is given elsewhere [18].

3 Computational model

The unsteady, three-dimensional mass continuity and momentum equations are solved using the finite volume method implemented on a graphics processing unit (GPU) for fast computation in the in-house code CUFLOW, as described in previous recent studies with this model [12, 20–22]. The flow phenomena too small to be captured by the grid spacing are modeled with the coherent-structure Smagorinsky model (CSM) sub-grid scale (SGS) model [23]. The applied magnetic field generates an electric current and Lorentz forces in the molten metal, which are found by solving a coupled set of three-dimensional magneto-hydro-dynamics (MHD) equations using the electric potential formulation. The MHD equations for charge conservation, current density, Poisson equation for electric potential, and Lorentz force are described elsewhere [14]. The applied magnetic field can simply be measured without flowing metal, as the relative magnitude of the induced field is negligible [6].

The model was used to simulate the two measured cases of the previous section, where a single-ruler EMBr magnetic field was applied through the thickness of the 1/6-scale liquid – GaInSn caster model with conductive side walls: The computational domain included both the liquid metal (for fluid flow and MHD equations), and the conductive side walls that represent the solidifying steel shell in the real caster (MHD equations only).

A free-slip boundary condition was applied on the top free surface of the mold. At the solid walls, the wall-function model of Werner and Wengle [24] was adopted, and a convective flow boundary condition was applied at the outlets [22]. An insulated electrical boundary condition (zero potential gradient) was applied by default to the outermost boundary of the metal side walls, to simulate air in the physical model, or the non-conducting mold slag layer that surrounds the solid steel shell in the real caster.

The mesh had 7.6 million brick cells and both simulations were started with zero initial velocity and the magnetic field was applied after 10 s of simulation time (200,000 time steps). The flow field was allowed to develop for 5 s before starting to collect the time averages, and time-averaged quantities and power spectra were then collected for 13 s. Ten days of computation were required for each simulation on a NVIDIA C2075 GPU with 1.15 GHz cuda-core frequency and 6 GB memory.

3.1 Comparison of simulations and measurements

The UDV measurements in the GaInSn physical model and the LES model predictions of the time-averaged flow pattern are compared in Figures 3–7. The two methodologies agree very well with each other and produce the same insights, so are presented together in this section.

Figure 3 shows contour plots of the time-averaged horizontal velocity. The top row is for 92-mm EMBr and the lower plot is for 121-mm EMBr. The first two columns compare the UDV measurements with the CUFLOW predictions, obtained by averaging data across the same ten horizontal lines. An excellent match is observed for both simulations, both qualitatively and quantitatively. The third column (right) shows the same CUFLOW results, with improved vertical resolution using all of the computational grid points. The jet exhibits a realistic continuous high-velocity region, which demonstrates that the two isolated regions of high velocity in each jet in the low-resolution middle-column plots are graphical artifacts. This agrees with previous findings [14].

The ruler magnetic field is known to deflect the jet upward [12] so the steeper, more downward-angled jet observed with lowering the ruler field from 92 to 121 mm is expected in Figure 3. Recirculation regions are seen just above and below the jet (negative velocity – blue – implies flow toward the narrow face). The strongest recirculating flow (red) is seen above the jet, especially with 92 mm. This recirculation was found in previous work [14] to be even stronger with insulated walls and was not present at all in this part of the mold with no EMBr.

Figures 4 and 5 compare the measured and calculated time-averaged horizontal velocities on three horizontal lines, 90, 100, and 110 mm from the free surface (corresponding to the fourth, fifth, and sixth sensors) for the two cases. The model results closely match the

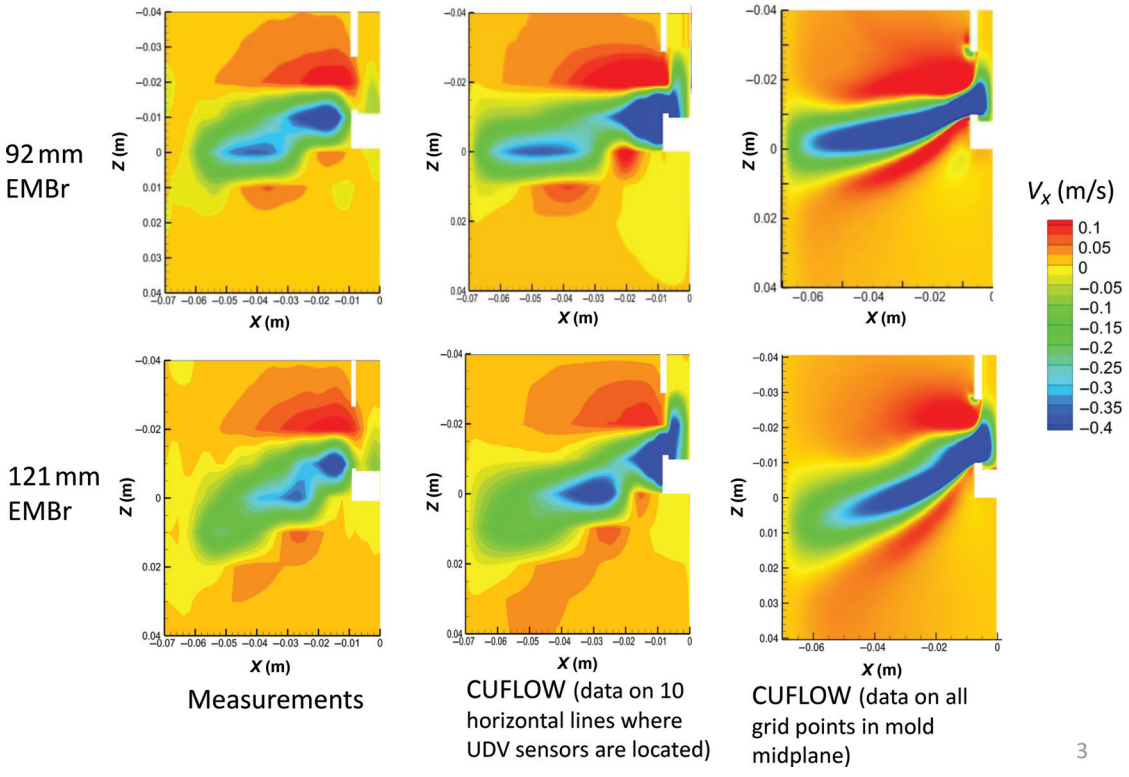

Figure 3: Experimental and modeled contours of time-averaged horizontal velocity, (V_x).

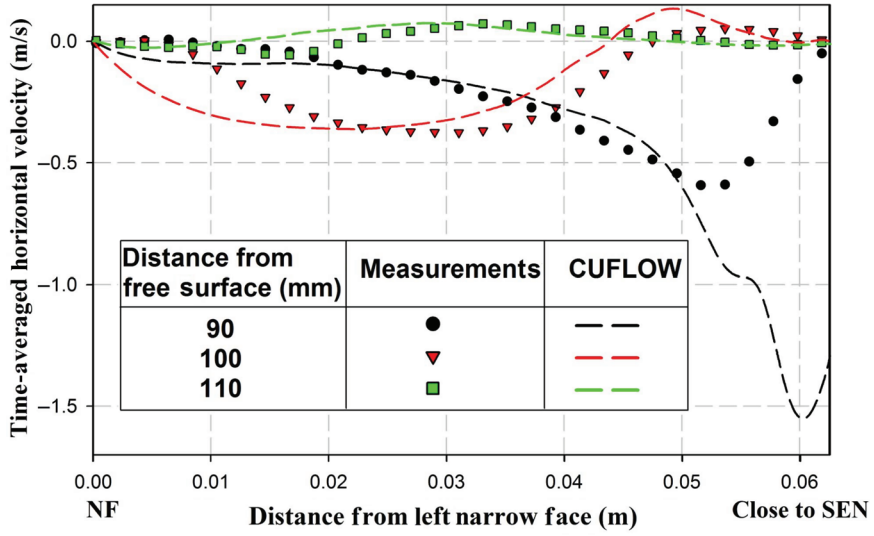

Figure 4: 92 mm EMBr – time-averaged horizontal velocity (V_x) profile on three lines across mold.

measurements, except for close to the SEN and narrow face walls, where the UDV measurements are diminished by interaction of the ultrasonic beam with these solid surfaces [11, 22, 25]. Because its jet is angled more steeply downward, so is lower, the maximum velocity along the line is found closer to the SEN ports for the 121 mm case.

The transient horizontal velocities measured by the UDV probes are compared to the CUFLOW simulations at two points indicated in Figure 1(a) and (d). Results at point E1 in the jet region $x = -41\,\text{mm}, y = 0\,\text{mm}, \text{z} = 0\,\text{mm})$ are in Figure 6, and results at point E4 located 40 mm higher above the jet are in Figure 7. In order to match the

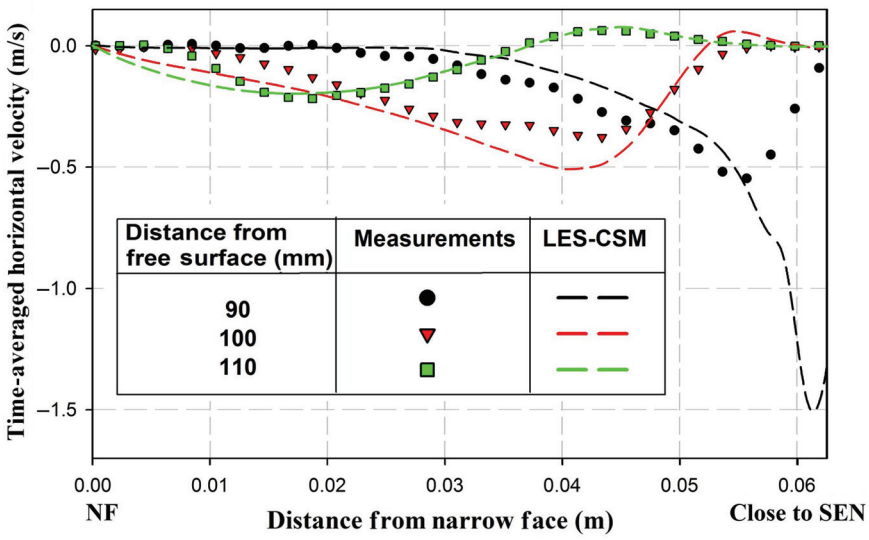

Figure 5: 121-mm EMBr – time-averaged horizontal velocity (V_x) profile on three lines across mold.

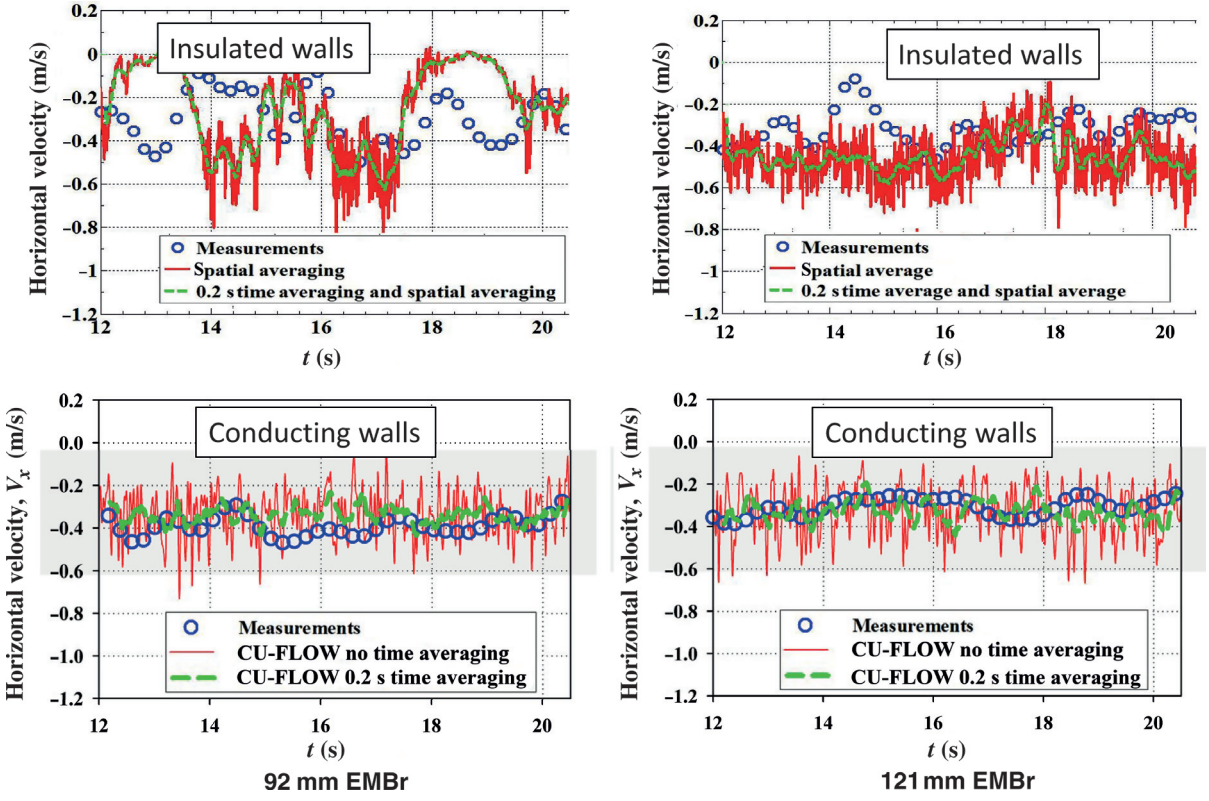

Figure 6: Transient history of *x*-velocity component at point E1 in the jet.

conditions of the transient measurements closely, a 0.2 second time average was performed on the calculated signal to match the response frequency (5 Hz) of the measuring sensors [22]. The measured and the time-averaged signals match well at both points for all cases.

Inside the jet, the left column in Figure 6 shows that the 92-mm ruler across the nozzle ports causes large-scale flow variations, which are much larger with insulated walls. Jet velocity at point E1 varies from 0 to 0.6 m/s with insulated walls with a time scale of several seconds.

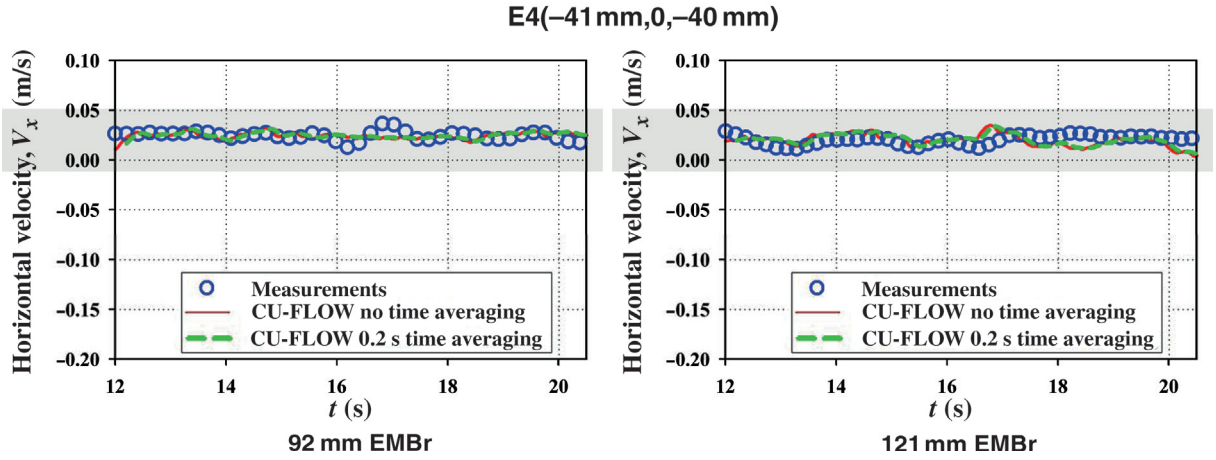

Figure 7: Transient history of *x*-velocity component at point E4 above the jet.

The variations decrease to 0.2 to 0.5 m/s with conducting walls. Lowering the ruler to 121 mm causes the variations to decrease, especially with insulated walls.

Above the jet, at point E4, Figure 7 shows that the velocity signal is much more stable. Both measurement and simulation show that the velocity variations drop from a maximum of ~0.03 m/s to less than ~0.025 m/s.

3.2 Nozzle flow

Contours of the time-averaged flow near the nozzle ports are compared in Figure 8 for the two cases of this study and with previous results without EMBr [14]. The ruler magnetic field pushes upward on the bottom of the jet, thereby making the jet thinner (less vertical spreading), and deflecting the jet toward horizontal. Thus, there is a natural progression of increasing downward jet angle exiting the ports (from ~20° to ~30° to ~40°), as the ruler field is lowered from across the ports (92 mm) to below the ports (121 mm) to the no-EMBr case.

3.3 Mold flow

Contours of time-averaged and instantaneous velocity magnitude are plotted in the mold in Figure 9. The flow patterns are quite symmetrical for both cases, which indicates that the simulation time was sufficient to achieve a reliable time average.

The magnetic field greatly changes the flow, which is generally a classic double-roll flow pattern, as discussed

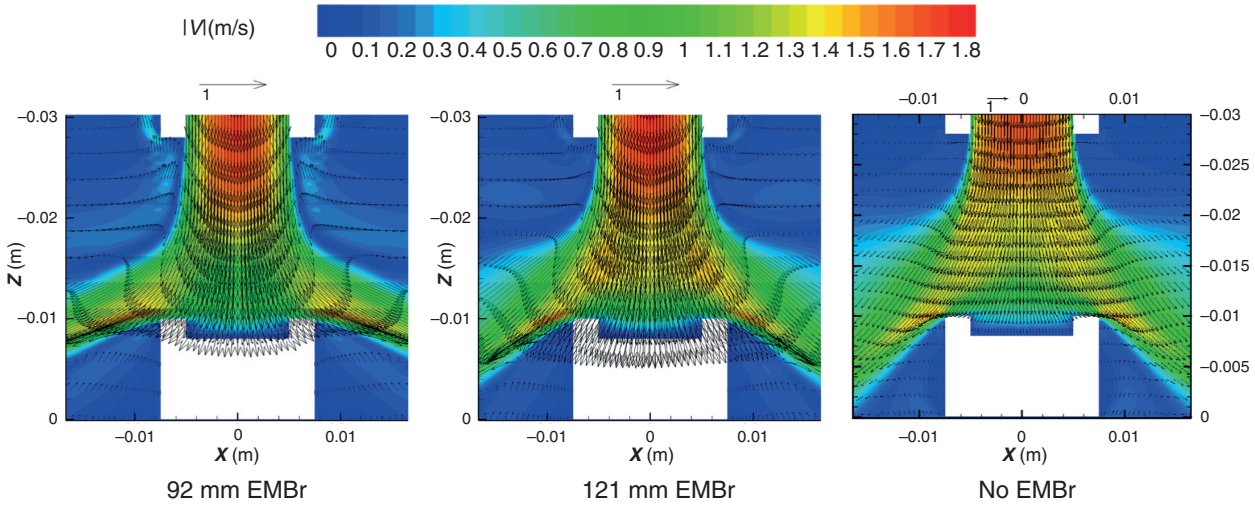

Figure 8: Time-averaged flow through the nozzle ports, showing effect of EMBr position on speed contours with vectors.

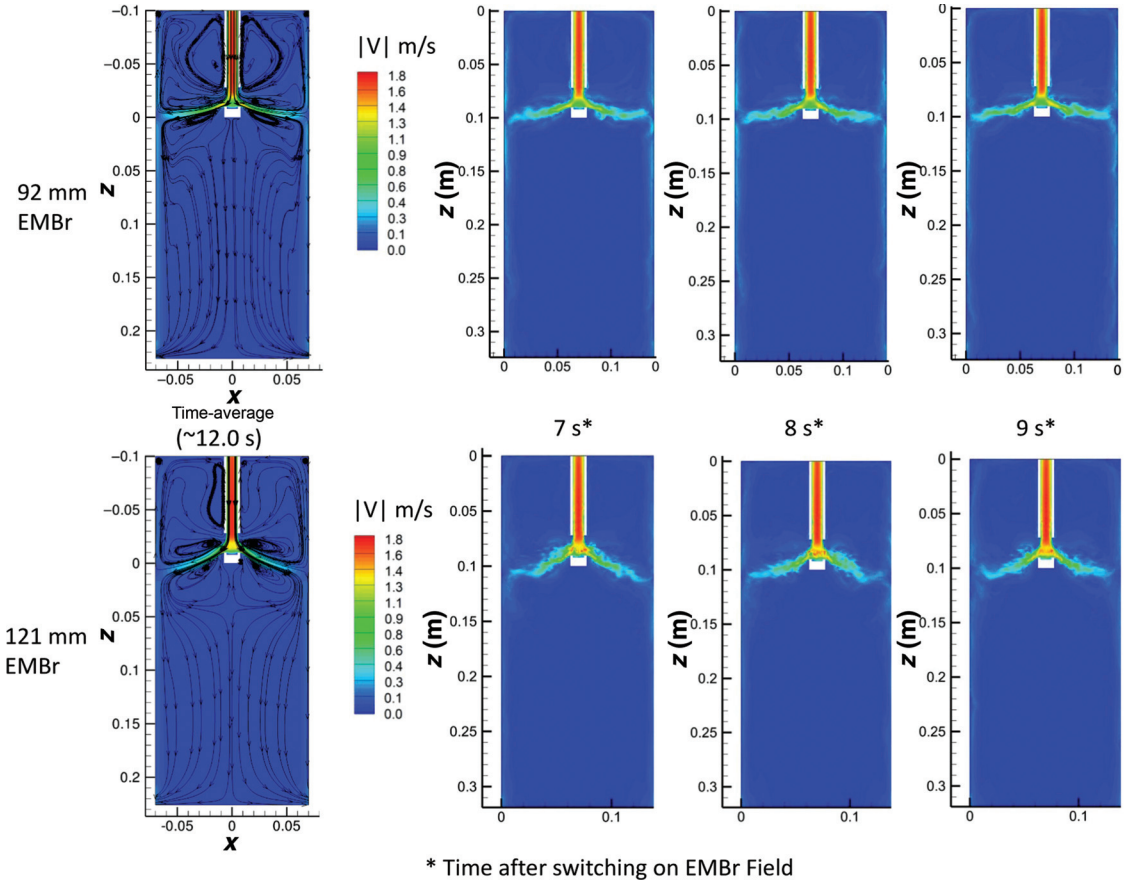

Figure 9: Flow in the mold, showing time-averaged and instantaneous speed contours.

elsewhere [14, 15]. Small elongated recirculation regions are found just and below both jets. Lowering the position of the ruler field caused less upward deflection of the jet, leading to slower flow in the upper region above the jets.

Flow across the top surface from the narrow face toward the SEN is slower as well with the 121 mm field.

In the lower region below the jet, the flow is almost uniform downward until splitting toward the two outlets at the bottom sides. This flow feature produced by the magnetic field contrasts with the two large recirculation zones experienced as a classic double-roll pattern without EMBr.

3.4 Surface flow

Many defects in continuous casting arise due to problems with surface flow. Flow across the top surface is generally from the narrow face toward the SEN for both simulations, as expected for a double-roll flow pattern. The flow is generally slow, owing to the deep submergence used in the GaInAs model. Due to its greater upward deflection of the jet, surface flow is faster with the higher 92 mm field, relative to the 121 mm field, as shown in Figure 10. The surface turbulence is greater with the 92 mm field as well, as shown in Figure 11. The higher turbulence is especially evident near the narrow-face meniscus region, where there is some reverse flow, observed in Figure 9. This higher turbulence is due to both the higher velocity of the surface flow, and to the greater flow instabilities, which accompany a field positioned across the nozzle, as discussed in the previous section. Surface turbulence is much higher for the case with insulated walls, which amplifies differences in flow stability [11–15].

4 Spectral analysis

Power spectrum analyses were performed for both the main two at points P1 and P2 in the jet region, and P4

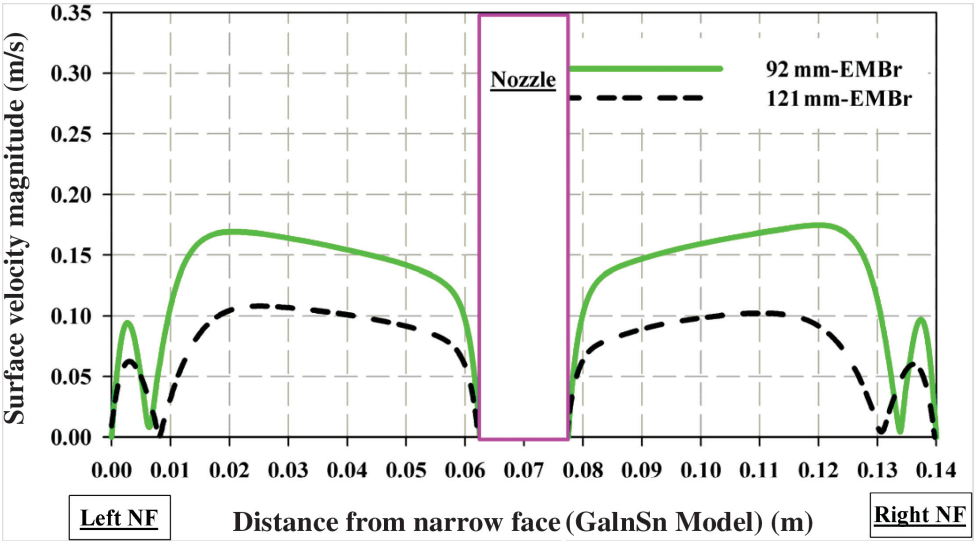

Figure 10: Horizontal velocity magnitude across top surface.

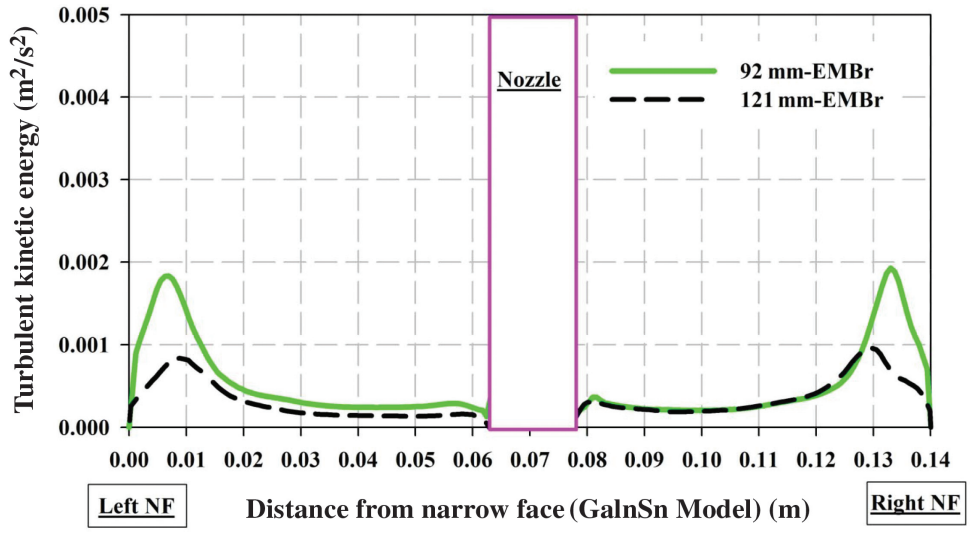

Figure 11: Kinetic energy across top surface.

near the top surface at the narrow face meniscus, as shown in Figures 12 and 13. The frequency domain is resolved from ~0.1 Hz to 10 kHz. The lowest frequency is limited by the total data collection time during the simulation of 13 s (~0.075 Hz). The highest frequency resolved with fast Fourier transform (FFT) is half of the signal sampling rate, which was 20 kHz for the 5×10^{-5} s time step size.

Magnetic fields are known to suppress turbulent flow fluctuations, especially at higher frequencies [12, 15]. This is evident in Figure 12 at point P1 inside the nozzle, where the stronger field from the higher 92 mm field lowers the turbulence at all frequencies, compared with the 121 mm case. After exiting the nozzle, at point P2, the power of the turbulent fluctuations becomes similar between the two cases. This is because the field centered over the nozzle tends to split the flow either upward or downward according to minute local variations, so this amplifies the variations. With the field below the nozzle, the jet is deflected more consistently upward, which leads to more flow stability.

The variations persist as the jet impinges upon the narrow face wall, and flows up toward the top surface. At point P4, in a small recirculation region near the top

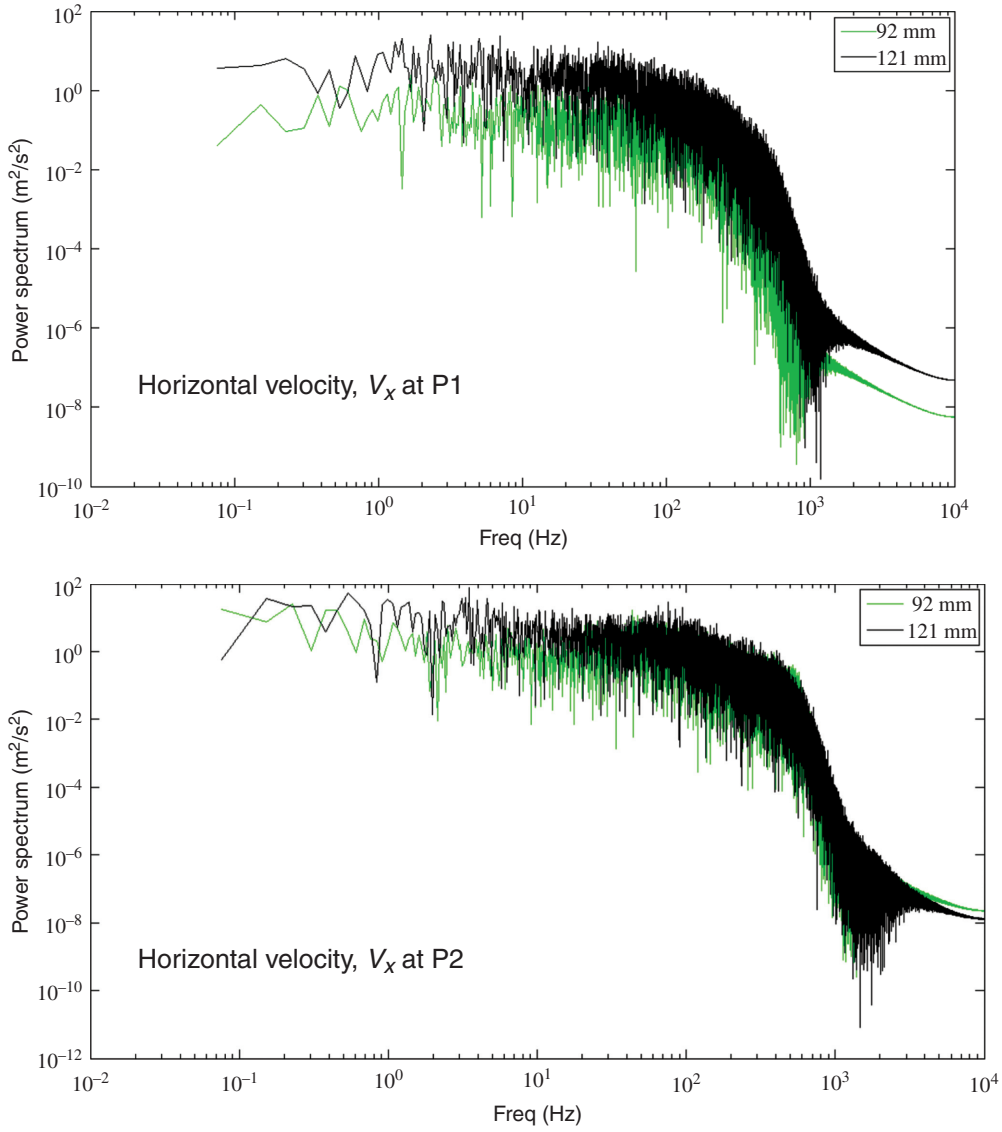

Figure 12: Power spectra of horizontal velocity at points inside nozzle (P1) and just outside nozzle ports (P2).

surface corner at the narrow face meniscus, Figure 13 shows the power spectra for both the horizontal and vertical velocity components. The 92 mm case has higher power fluctuations at all frequencies, showing that the flow is more unstable than the lower configuration. This effect is consistent with previous work with insulated walls, which shows that positioning the maximum magnetic field across the nozzle ports produces severe instability. The instability is less severe in the present work with conducting walls, but still demonstrates the benefit of controlling nozzle submergence and EMBr ruler field positioning to avoid aligning the maximum field strength across the nozzle ports.

5 Conclusions

EMFs are an important method to control transient fluid flow, stability, and thereby steel quality in the mold region of continuous slab casting processes. The transient flow in a typical steel slab caster is investigated with a low-melting liquid metal GaInSn alloy is a scaled physical model with conducting walls to represent the solidifying steel shell, using both UDV measurements and LESs with in-house code, CUFLOW. Flow behavior is compared for two different vertical positions of a single-ruler magnetic field, centering the maximum field strength either across or just below the bifurcated nozzle ports. UDV

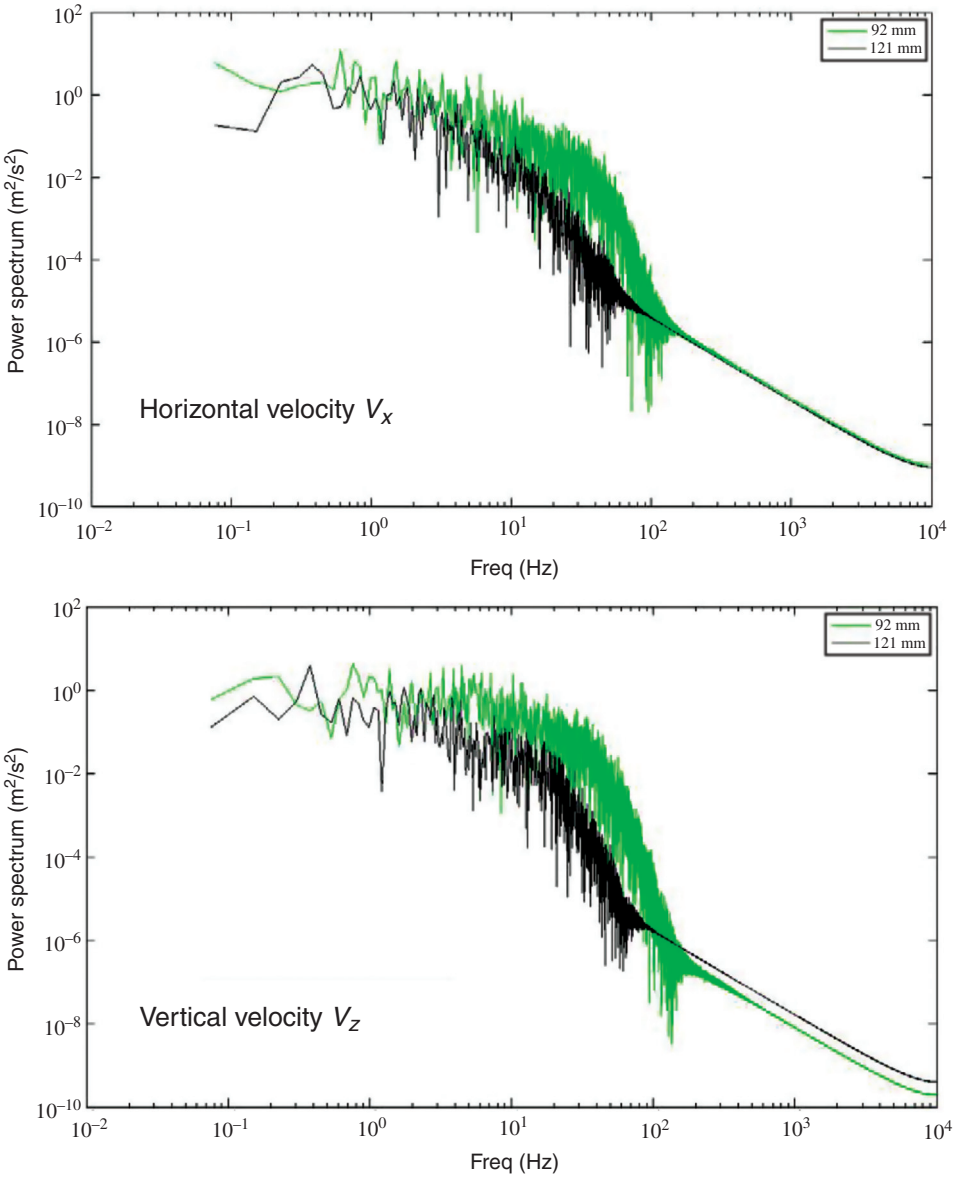

Figure 13: Power spectra of two main velocity components at point P4 (–65.83, 0, –99.0 mm) at top surface near narrow face.

measurements of horizontal velocity are conducted in the jet region and revealed the complex interaction of the static magnetic field with the mold flow. The simulations resolve the important transient behaviors, using grids of over 5-million cells with a fast parallel solver.

The agreement of the LES model predictions with the UDV measurements is remarkable. So long as the predictions are filtered and plotted the same way as the measurements, the model can capture quantitatively both the time-averaged and transient flow behavior.

Both investigation methods together reveal consistent new insights into the effect of EMBr single-ruler magnetic field on both the flow pattern and its stability.

1. The magnetic field alters the generally classic double-roll flow pattern for all conditions studied.
2. Both ruler-magnetic fields defect the flow more horizontally and upward toward the surface, producing higher surface velocities, especially when the field is oriented across the nozzle.
3. Lowering the ruler field below the ports allows steeper downward jet angles into the mold and leads to lower surface velocity, and lower surface kinetic energy for the conditions of this study.
4. Applying the EMBr ruler field directly across the nozzle ports worsens the flow stability, producing strong unbalanced, asymmetric transient behavior and complex flow.

5. Lowering the field below the ports stabilizes the flow, giving less unbalanced flow behavior.
6. Relative to insulated walls, the flow stability problems with realistic conducting walls have similar trends, but are lessened greatly.

The practical implication of this work is that commercial operations should control submergence depth and magnetic field position together to avoid maximum field strength across the nozzle ports.

Acknowledgments: This work was supported by the National Science Foundation Grant CMMI 11–30882 and the Continuous Casting Consortium at the University of Illinois at Urbana-Champaign. We also acknowledge the NVIDIA Professor Partnership grant for providing us the Fermi GPU cards, which enabled the GPU modeling. Finally, we acknowledge the financial support from the German Helmholtz Association in the framework of the LIMTECH alliance, which enabled the experimental measurements conducted at HZDR.

References

1. Thomas BG. Fluid flow in the mold, Chapter 14. In: Cramb, A, editor. Making, shaping and treating of steel, 11th ed., vol. 5, Casting Volume. Pittsburgh, PA: AISE Steel Foundation, 2003:14.1–14.41.
2. Kunstreich S, Dauby PH. Effect of liquid steel flow pattern on slab quality and the need for dynamic electromagnetic control in the mould. Ironmaking Steelmaking 2005;32:80–6.
3. Idogawa A, Sugizawa M, Takeuchi S, Sorimachi K, Fujii T. Control of molten steel flow in continuous casting mold by two static magnetic fields imposed on whole width. Mat Sci Eng A 1993;173:293–7.
4. Zeze M, Harada H, Takeuchi E, Ishii T. Application of DC magnetic-field for the control of flow in the continuous-casting strand. 76th Steelmaking Conference Proceedings, 1993, vol. 76: 267–272.
5. Miki Y, Takeuchi S. Internal defects of continuous casting slabs caused by asymmetric unbalanced steel flow in mold. ISIJ Int 2003;43:1548–55.
6. Cukierski K, Thomas BG. Flow control with local electromagnetic braking in continuous casting of steel slabs. Metall Mater Trans B 2008;39:94–107.
7. Kim D, Kim W, Cho K. Numerical simulation of the coupled turbulent flow and macroscopic solidification in continuous casting with electromagnetic brake. ISIJ Int 2000;40:670–6.
8. Takatani K, Nakai K, Kasai N, Watanabe T, Nakajima H. Analysis of heat transfer and fluid flow in the continuous casting mold with electromagnetic brake. ISIJ Int 1989;29:1063–8.
9. Ha MY, Lee HG, Seong SH. Numerical simulation of three-dimensional flow, heat transfer, and solidification of steel in continuous casting mold with electromagnetic brake. J Mater Process Technol 2003;133:322–39.
10. Harada H, Toh T, Ishii T, Kaneko K, Takeuchi E. Effect of magnetic field conditions on the electromagnetic braking efficiency. ISIJ Int 2001;41:1236–44.
11. Timmel K, Eckert S, Gerbeth G. Experimental investigation of the flow in a continuous-casting mold under the influence of a transverse, direct current magnetic field. Metall Mater Trans B 2011;42:68–80.
12. Chaudhary R, Thomas BG, Vanka SP. Effect of electromagnetic ruler braking (EMBr) on transient turbulent flow in continuous slab casting using large eddy simulations. Metall Mater Trans B 2012;43:532–53.
13. Miao X, Timmel K, Lucas D, Ren S, Eckert Z, Gerbeth G. Effect of an electromagnetic brake on the turbulent melt flow in a continuous-casting mold. Metall Mater Trans B 2012;43:954–72.
14. Singh R, Thomas BG, Vanka SP. Effects of a magnetic field on turbulent flow in the mold region of a steel caster. Metall Mater Trans B 2013;44:1201–21.
15. Singh R, Thomas BG, Vanka SP. Large eddy simulations of double-ruler electromagnetic field effect on transient flow during continuous casting. Metall Mater Trans B 2014;45:1098–115.
16. Li B, Okane T, Umeda T. Modeling of molten metal flow in a continuous casting process considering the effects of argon gas injection and static magnetic-field application. Metall Mater Trans B 2000;31:1491–503.
17. Cho S-M, Kim S-H, Thomas BG. Transient fluid flow during steady continuous casting of steel slabs, part II: effect of double-ruler electro-magnetic braking (EMBr). ISIJ Int 2014;54:855–64.
18. Timmel K, Wondrak T, Roder M, Stefani F, Eckert S, Gerbeth G. Use of cold liquid metal models for investigations of the fluid flow in the continuous casting process. Steel Res Int 2014;85:1283–90.
19. Plevachuk Y, Sklyarchuk V, Eckert S, Gerbeth G, Novakovic R. Thermophysical properties of the liquid Ga-In-Sn eutectic alloy. J Chem Eng Data 2014;59:757–63.
20. Chaudhary R, Vanka SP, Thomas BG. Direct numerical simulations of magnetic field effects on turbulent flow in a square duct. Phys Fluids 2010;22:75102–15.
21. Chaudhary R, Shinn AF, Vanka SP, Thomas BG. Direct numerical simulations of transverse and spanwise magnetic field effects on turbulent flow in a 2:1 aspect ratio rectangular duct. Comput Fluids 2011;51:100–14.
22. Chaudhary R, Ji C, Thomas BG, Vanka SP. Transient turbulent flow in a liquid-metal model of continuous casting, including comparison of six different methods. Metall Mater Trans B 2011;42B:5987–1007. doi:10.1007/s11663-011-9526-1
23. Kobayashi H. Large eddy simulation of magnetohydrodynamic turbulent channel flows with local subgrid-scale model based on coherent structures. Phys Fluids 2006;18:045107.
24. Werner H, Wengle H. Large-eddy simulation of turbulent flow over and around a cube in a plate channel. In 8th Symposium on Turbulent Shear Flows, 1991:155–68.
25. Timmel K, Eckert S, Gerbeth G, Stefani F, Wondrak T. Experimental modeling of the continuous casting process of steel using low melting point metal alloys-the LIMMCAST program. ISIJ Int 2010;50:1134–41.